arXiv:cond-mat/9907238v1 [cond-mat.dis-nn] 16 Jul 1999

Scattering of plane-wave atomic vibrations in disordered structures

S.N.Taraskin and S.R.Elliott

Department of Chemistry, University of Cambridge, Lensfield Road, Cambridge CB2 1EW, UK

(to be published in the Proceedings of the summer school (Cargese, 1999): *Physics of Glasses: Structure and Dynamics*, Eds. P. Jund and R. Jullien)

Abstract. A theoretical analysis of the scattering of plane-wave atomic excitations in disordered solids has been made in terms of the spectral densities. Hybridization between transverse and longitudinal waves of approximately the same frequency is demonstrated. The analytic results agree well with the results obtained from computer simulation for a toy linear zig-zag chain model and a model of vitreous silica constructed by molecular dynamics.

I INTRODUCTION

Propagation of classical plane waves in random scattering media has attracted a lot of theoretical and experimental attention in recent years [1,2]. The phenomena of wide interest include weak localization [1,2], Anderson localization [3], phonon localization [4–6] and related behaviour of plane waves in the Ioffe-Regel crossover region [7] separating weakly and strongly scattered waves [8,9].

Vibrational plane waves propagate well in disordered structures in the long-wavelength limit, $ka \ll 1$, with k the wavevector and a a measure of the microscopic scale of the structure (being of the order of interatomic distances), when the atomic structure behaves as an elastic continuum and disorder on the microscopic level is not of great importance. The situation is changed with decreasing wavelength and, on the microscopic scale, disorder becomes important and the wavevector is no longer a good quantum value [10–17].

In the investigation of the propagation of the plane-wave vibrational excitations in disordered structures, different decay channels have been suggested to explain their attenuation: (i) disorder-induced channels [18–22], (ii) anharmonic channels [20] and (iii) channels involving two-level systems [23–26]. The anharmonic channels are strongly enhanced with increasing temperature, particularly at temperatures comparable with the glass-transition temperature, $T_{\rm g} \sim 10^3$K. In

contrast, scattering by two-level systems can be important at low temperatures [25], $T \ll T_{\rm TLS} \sim 10 - 100$K [24,27]. In the intermediate temperature range, $T_{\rm TLS} \leq T \ll T_{\rm g}$, which is considered below, the scattering processes involving two-level systems are suppressed and the atomic dynamics are usually harmonic [21,28], meaning that disorder-induced channels play the most important role in the decay mechanism of plane-wave excitations.

If the harmonic approximation is valid for describing the atomic dynamics, then a normal-mode analysis can be used for the problem under consideration. The normal modes can be found either analytically or numerically. A general theory of atomic vibrations in disordered structures, which in principle should result in normal modes, has been mainly developed for particular simple model structures [18,29–34], which can hardly describe quantitatively the situation in real structures. Therefore, a numerical approach could be very useful in the calculation of normal modes, e.g. by direct diagonalization of the dynamical matrix which can be available, e.g. from molecular dynamics simulations.

The main questions we address in this paper are: how are plane-wave vibrational excitations scattered by disorder and what are the characteristics of the final state after scattering?

Our approach to the problem is based on combining analytical and numerical techniques. First, we create a few structural models of a disordered atomic material: (i) realistic models of v-SiO_2 using molecular dynamics and (ii) toy models of a linear zig-zag chain. Then all eigenmodes and eigenfrequencies (in the harmonic approximation) are found numerically. These characteristics fully determine the dynamical response of the system (and final state at $t \to \infty$) to any external excitations, including the plane-wave excitations of present interest. The final state after scattering was investigated then in momentum space (analytically and numerically).

II FORMALISM

The time evolution of any vibrational excitation is fully determined in the harmonic approximation by the eigenmodes and eigenfrequencies of the system. Indeed, the initial excitation can be expanded in the eigenmodes, the time dependence of which is known. The coefficients in such an expansion are defined by the shape of the initial vibrational excitation. Here we consider only plane-wave external initial excitations, mainly because exactly such excitations are generated in a system by inelastic neutron, light and electron scattering [35].

In amorphous materials, because of disorder, the eigenmodes are not plane waves even in the long-wavelength limit. Therefore, an initial plane wave, when expanded over eigenmodes, contains different eigenmodes characterized by different weights in this expansion. The eigenmodes participating in the expansion evolve differently with time, so that the propagating excitation becomes different in shape compared with the initial one. If we expand the vibrational state in plane waves after a certain

time, then this expansion contains not only the initial plane-wave component but also other plane waves characterized by different wavevectors. This means that the initial plane wave is scattered by the structure into a different final state. Our aim here is to study the properties of the final state after decay, for different wavevectors of an initial plane wave.

Let us consider an external wave excitation introduced in the system, $\mathbf{u}(t)$, which at the initial moment of time is an ideal plane wave, $\mathbf{w_k}$, characterized by the wavevector $\mathbf{k}$, unit polarization vector $\hat{\mathbf{n}}$ and initial phase ϕ_0:

$$\mathbf{u}(t=0) = \mathbf{w_k} \equiv A\hat{\mathbf{n}}\cos[\mathbf{k}\cdot\mathbf{r} + \phi_0] \ , \tag{1}$$

where $\mathbf{u}$ is a $3N$-dimensional displacement vector, the i-th component of which describes the displacement of atom i from its equilibrium position at $\mathbf{r_i}$, A is the normalization constant defined below and the wavevector index $\mathbf{k}$ includes also the polarization index $\hat{\mathbf{n}}$. In our analytical treatment, we assume that eigenmodes and eigenfrequencies are known, e.g. from numerical simulations. The initial displacement vector, Eq. (1), each atomic component of which is multiplied by the mass factor $m_i = M_i N/\sum_i M_i$ (M_i stands for the mass of atom i) can be expanded in eigenmodes as:

$$\mathbf{u}(0) = \sum_{j=1}^{3N} \overline{\alpha}^j_{\mathbf{k}} \mathbf{e^j}/\sqrt{m} \ , \tag{2}$$

where the symbolic script $\mathbf{e^j}/\sqrt{m}$ means that each i-th component of vector $\mathbf{e^j}$ is divided by the factor $\sqrt{m_i}$. The coefficients $\overline{\alpha}^j_{\mathbf{k}}$ in expansion (2), the squares of which are the spectral densities of the system, are defined by the following equation:

$$\overline{\alpha}^j_{\mathbf{k}} = \langle \mathbf{e}^j \cdot \sqrt{m}\mathbf{u_k} \rangle \equiv \sum_{i=1}^{N} \sqrt{m_i}\mathbf{e}^j_i \cdot \mathbf{w}_{\mathbf{k},i} \ . \tag{3}$$

The spectral-density coefficients, Eq. (3), fully determine the dynamical response of the system to plane-wave excitation. Indeed, at any moment of time t, the displacement vector of the propagating excitation can be represented via eigenmodes developing in time as:

$$\mathbf{u}(t) = \sum_{1}^{3N} \overline{\alpha}^j_{\mathbf{k}} \frac{\mathbf{e}^j}{\sqrt{m}} \cos\omega_j t \ . \tag{4}$$

For the sake of simplicity and without loss of generality (as shown below), we consider the initial excitation to be a standing wave, i.e. $\dot{\mathbf{u}}(0) = 0$, leading to the absence of terms proportional to $\sin\omega_j t$ in expression (4). It is convenient for the initial vector $\sqrt{m}\mathbf{u_k}(0)$ to be normalized to unity, so that

$$\sum_{1}^{3N} |\overline{\alpha}^j_{\mathbf{k}}|^2 = 1 \ , \tag{5}$$

and the normalization constant in Eq. (1) is $A^2 = [\sum_i m_i |\mathbf{u}_\mathbf{k}(0)|^2]^{-1}$.

An ideal initial plane wave (1) scatters with time to different plane waves. In order to calculate the weights of different plane-wave components in the propagating excitation, we expand the displacement vector $\mathbf{u}(t)$ in plane waves:

$$\mathbf{u}(t) = \sum_{\mathbf{k}'} \mathbf{u}_{\mathbf{k}'}(t) \ , \tag{6}$$

where the sum is taken over all wavevectors $\mathbf{k}'$ (allowed by the periodic simulation box in the case of a finite model) and all polarizations (two transverse and one longitudinal for each wavevector), and the waves $\mathbf{u}_{\mathbf{k}'}(t)$ are defined as:

$$\mathbf{u}_{\mathbf{k}'}(t) = a_{\mathbf{k}'}(t) A \hat{\mathbf{n}}' \cos\left(\mathbf{k}' \cdot \mathbf{r} + \phi_{\mathbf{k}'}(t)\right) \ . \tag{7}$$

The same normalization as in Eq. (1) is used here. In order to find the time dependence of the amplitude $a_{\mathbf{k}'}(t)$ and phase $\phi_{\mathbf{k}'}(t)$, it is convenient to rewrite Eq. (7) in the following form:

$$\mathbf{u}_{\mathbf{k}'}(t) = a_{\mathbf{k}',\mathrm{c}}(t) \mathbf{w}_{\mathbf{k}',\mathrm{c}} + a_{\mathbf{k}',\mathrm{s}}(t) \mathbf{w}_{\mathbf{k}',\mathrm{s}} \ , \tag{8}$$

where

$$\mathbf{w}_{\mathbf{k}',\mathrm{c}} = A \hat{\mathbf{n}}' \cos \mathbf{k}' \cdot \mathbf{r} \quad \text{and} \quad \mathbf{w}_{\mathbf{k}',\mathrm{s}} = A \hat{\mathbf{n}}' \sin \mathbf{k}' \cdot \mathbf{r} \ , \tag{9}$$

so that

$$a_{\mathbf{k}'}(t) = (a^2_{\mathbf{k}',\mathrm{c}}(t) + a^2_{\mathbf{k}',\mathrm{s}}(t))^{1/2} \ , \tag{10}$$

$$\phi_{\mathbf{k}'}(t) = \mathrm{Arctan}[a_{\mathbf{k}',\mathrm{s}}(t)/a_{\mathbf{k}',\mathrm{c}}(t)] \ . \tag{11}$$

The coefficients $a_{\mathbf{k}',\mathrm{c(s)}}(t)$ before the cos- (sin-) like components in Eq. (8) can be found by multiplying both sides of this equation by $\mathbf{w}_{\mathbf{k}',\mathrm{c(s)}}$ and using Eq. (3), so that

$$a_{\mathrm{k}',\mathrm{c(s)}}(t) = \sum_j \overline{\alpha}^j_{\mathbf{k}} \underline{\alpha}^j_{\mathbf{k}',\mathrm{c(s)}} \cos \omega_j t / \langle \mathbf{w}^2_{\mathbf{k}',\mathrm{c(s)}} \rangle \ . \tag{12}$$

where

$$\langle \mathbf{w}^2_{\mathbf{k}',\mathrm{c(s)}} \rangle \equiv \sum_{i=1}^{N} |(\mathbf{w}_{\mathbf{k}',\mathrm{c(s)}})_i|^2 \ . \tag{13}$$

The spectral-density coefficients $\underline{\alpha}^j_{\mathbf{k}',\mathrm{c(s)}}$ for plane waves of cos- and sin-like type are defined by the following equation:

$$\underline{\alpha}^j_{\mathbf{k},\mathrm{c(s)}} = \langle \mathbf{e}^j \cdot \frac{1}{\sqrt{m}} \mathbf{w}_{\mathbf{k},\mathrm{c(s)}} \rangle \equiv \sum_{i=1}^{N} \frac{1}{\sqrt{m_i}} \mathbf{e}^j_i \cdot (\mathbf{w}_{\mathbf{k},\mathrm{c(s)}})_i \ . \tag{14}$$

The spectral-density coefficients $\underline{\alpha}^j_{\mathbf{k},\mathrm{c(s)}}$ in a multicomponent system, in contrast to $\overline{\alpha}^j_{\mathbf{k}}$, instead of being normalized to unity are normalized by the following value:

$$\sum_{j=1}^{3N} |\underline{\alpha}^j_{\mathbf{k},\mathrm{c(s)}}|^2 = \frac{\sum_i (m_i)^{-1} |\mathbf{w}_{\mathbf{k},\mathrm{c(s)}}|^2}{\sum_i m_i |\mathbf{w}_{\mathbf{k},\mathrm{c(s)}}|^2} \ , \tag{15}$$

having the value $\simeq 0.7$ in the case of vitreous silica.

Eqs. (10) - (15) fully determine the time evolution of different $\mathbf{k}'$ plane-wave components in the propagating vibrational excitation via the spectral densities and the vibrational spectrum itself. Another useful characteristic often used to characterize the decay of an initial external excitation is the time correlation function [36],

$$\frac{\langle \mathbf{u}(t) \cdot \mathbf{u}(0) \rangle}{\langle \mathbf{u}(0) \cdot \mathbf{u}(0) \rangle} \equiv \frac{\sum_i \mathbf{u}_i(t) \mathbf{u}_i(0)}{\sum_i \mathbf{w}_{\mathbf{k},i} \mathbf{w}_{\mathbf{k},i}} = \frac{\sum \overline{\alpha}^j_{\mathbf{k}} \underline{\alpha}^j_{\mathbf{k}} \cos \omega_j t}{\langle \mathbf{w}^2_{\mathbf{k}} \rangle} \ , \tag{16}$$

where the spectral-density coefficient $\underline{\alpha}^j_{\mathbf{k}}$ is defined by Eq. (14) with $\mathbf{w}_{\mathbf{k},\mathrm{c(s)}}$ replaced by $\mathbf{w}_{\mathbf{k}}$, and is related to the spectral-density coefficient $\overline{\alpha}^j_{\mathbf{k}}$ according to the following equation:

$$\underline{\alpha}^j_{\mathbf{k}} = \sum_{j'} \overline{\alpha}^{j'}_{\mathbf{k}} \langle \mathbf{e}^j m^{-1} \mathbf{e}^{j'} \rangle \ . \tag{17}$$

In the case of a one-component system, the spectral-density coefficients $\underline{\alpha}^j_{\mathbf{k}}$ and $\overline{\alpha}^j_{\mathbf{k}}$ are obviously identical.

The decay of the external plane-wave excitation can also be characterized via the properties of the final state after decay, averaged over time as $t \to \infty$. An initial plane-wave excitation characterized by the wavevector $\mathbf{k}$ and polarization $\hat{\mathbf{n}}$ is scattered to different plane-wave components characterized by the wavevectors $\mathbf{k}'$ and polarizations $\hat{\mathbf{n}}'$. The distribution, $\rho(\mathbf{k}', \hat{\mathbf{n}}' | \mathbf{k}, \hat{\mathbf{n}})$, of the weights of different plane-wave components averaged over time in the final state, $\overline{a^2_{\mathbf{k}',\hat{\mathbf{n}}'}(t)}$, is of particular interest. Such a distribution is defined by the following equation:

$$\rho(\mathbf{k}', \hat{\mathbf{n}}' | \mathbf{k}, \hat{\mathbf{n}}) = \overline{a^2_{\mathbf{k}'}(t)} = \frac{1}{2} \left\{ \frac{\sum_j |\overline{\alpha}^j_{\mathbf{k}}|^2 |\underline{\alpha}^j_{\mathbf{k}',\mathrm{s}}|^2}{(\langle \mathbf{w}^2_{\mathbf{k}',\mathrm{s}} \rangle)^2} + \frac{\sum_j |\overline{\alpha}^j_{\mathbf{k}}|^2 |\underline{\alpha}^j_{\mathbf{k}',\mathrm{c}}|^2}{(\langle \mathbf{w}^2_{\mathbf{k}',\mathrm{c}} \rangle)^2} \right\} \ , \tag{18}$$

where, as in Eq. (1) and subsequently, the wavevector index $\mathbf{k}'$ also includes the polarization index $\hat{\mathbf{n}}'$. Eq. (18) is obtained by averaging Eq. (10) over time and using Eq. (12). Bearing in mind that $\langle \mathbf{w}^2_{\mathbf{k}',\mathrm{s}} \rangle \simeq \langle \mathbf{w}^2_{\mathbf{k}',\mathrm{c}} \rangle \simeq \langle \mathbf{w}^2_{\mathbf{k}'} \rangle$ and that the sum $|\underline{\alpha}^j_{\mathbf{k}',\mathrm{s}}|^2 + |\underline{\alpha}^j_{\mathbf{k}',\mathrm{c}}|^2$ is independent of the phase of cos- and sin-like components defined by Eq. (9), expression (18) can be transformed to:

$$\rho(\mathbf{k}', \hat{\mathbf{n}}' | \mathbf{k}, \hat{\mathbf{n}}) = \frac{\sum_j |\overline{\alpha}^j_{\mathbf{k}}|^2 |\underline{\alpha}^j_{\mathbf{k}'}|^2}{(\langle \mathbf{w}^2_{\mathbf{k}'} \rangle)^2} \ . \tag{19}$$

The distribution (19) averaged over all polarizations $\hat{\mathbf{n}}'$ in the final state is

$$\rho_{\rm av}(\mathbf{k}'|\mathbf{k},\hat{\mathbf{n}}) \simeq 2\rho(\mathbf{k}',\hat{\mathbf{n}}'_{\rm t}|\mathbf{k},\hat{\mathbf{n}}) + \rho(\mathbf{k}',\hat{\mathbf{n}}'_{\rm l}|\mathbf{k},\hat{\mathbf{n}}) \ , \tag{20}$$

where the unit vector $\hat{\mathbf{n}}'_{\rm t}$ stands for transverse polarization in the final state while $\hat{\mathbf{n}}'_{\rm l}$ refers to longitudinal polarization, and the factor 2 takes into account the existence of two independent and, in glasses, equivalent transverse polarizations. Glasses are isotropic, and an averaging of Eqs. (18)-(20) over the directions of both initial and final wavevectors (including averaging over transverse polarizations in the initial wave) can be made, resulting in:

$$\rho_{\rm av,t(l)}(k'|k) = \langle \rho_{\rm av}(\mathbf{k}'|\mathbf{k},\hat{\mathbf{n}}_{\rm t(l)})\rangle_{\Omega_{\mathbf{k},\mathbf{k}'}} \ . \tag{21}$$

If we are interested in the contribution of the same plane-wave $\mathbf{k}$-component as in the initial excitation, then the wavevector $\mathbf{k}'$ should be replaced by $\mathbf{k}$ in Eqs. (18)-(20) and averaging only over $\mathbf{k}$-directions should be made in Eq. (21).

III SPECTRAL DENSITIES

As follows from Sec. II, the coefficients $\overline{\alpha}^j_{\mathbf{k}}$, $\underline{\alpha}^j_{\mathbf{k}}$ in the expansion of different $\mathbf{k}$-plane-waves over the eigenmodes, i.e. projections of plane waves onto eigenvectors, and related spectral densities, $|\underline{\alpha}^j_{\mathbf{k}}|^2$, $|\overline{\alpha}^j_{\mathbf{k}}|^2$ and $\overline{\alpha}^j_{\mathbf{k}}\underline{\alpha}^j_{\mathbf{k}}$, fully determine the dynamical response of the system to the initial plane-wave excitation. We calculate below the spectral densities for two models of disordered structures: (i) a model of v-SiO_2 constructed by molecular dynamics and (ii) a disordered zig-zag chain.

A Vitreous silica

The models of v-SiO_2 have been constructed by NPT-molecular-dynamics simulations, using the potential of van Beest [37]. The van Beest potential has been modified for small interatomic distances according to Guissani and Guillot [38]. At large interatomic distances, we have used a cutoff for short-range interactions, multiplying the modified van Beest potential by a Fermi-like step function. The step function is characterized by the step position at $R_{\rm cut} = 5.5\mathring{A}$ and the step width $\delta R_{\rm cut} = 0.5\mathring{A}$ for all atomic species. The latter cutoff has been used to obtain a density of the glassy structure (at zero pressure), of 2.38g/cm^3, reasonably close to the experimental value of 2.2g/cm^3 (see the discussion of the densification problem in Ref. [38]). Note that a similar cutoff ($R_{cut} = 5.0\mathring{A}$ and $\delta R_{cut} = 0$) has been used by Vollmayr *et al.* [39].

All glassy models have been created by quenching from the melt ($T = 6000$K) to the well-relaxed glassy state ($T \sim 10^{-4}$K) at an average quench rate of ~ 1K/ps. No coordination defects have been found in the models. The fully dense dynamical matrices for the relaxed systems were diagonalized directly, resulting in eigenvectors $\{\mathbf{e}^j\}$ and eigenvalues (ω_j), thus allowing us to perform a complete harmonic

vibrational analysis. Structural characteristics and vibrational properties of the models are very similar to those described in Ref. [40].

The models of v-SiO_2 were of two types: a cubic model containing $N = 1650$ atoms and of box length $L \simeq 28.4\mathring{A}$, and a bar configuration containing $N = 1500$ atoms of size $85.6\mathring{A} \times 15.6\mathring{A} \times 15.6\mathring{A}$ (a bar-shaped model of B_2O_3 has been also used in Ref. [41]). The bar-shaped models were constructed to allow access to much lower values of k ($\geq 0.07\mathring{A}^{-1}$) for modes propagating along the bar than can be obtained for the cubic models ($k \geq 0.22\mathring{A}^{-1}$).

Silica is a multicomponent system so that the three spectral densities differ from each other due to different contributions in the coefficients $\overline{\alpha}^j_{\mathbf{k}}$ and $\underline{\alpha}^j_{\mathbf{k}}$ of the mass factor (see Eqs. (3) and (14)). In the case of vitreous silica, the masses of the atomic species are quite comparable and the mass factor is of the order of unity, so that the different types of the spectral densities differ only slightly from each other and the following approximate relationships can be used: $|\underline{\alpha}^j_{\mathbf{k}}|^2 \simeq A_1|\overline{\alpha}^j_{\mathbf{k}}|^2$ and $\overline{\alpha}^j_{\mathbf{k}}\underline{\alpha}^j_{\mathbf{k}} \simeq A_2|\overline{\alpha}^j_{\mathbf{k}}|^2$, with the normalization constants for the corresponding spectral densities being $A_1 = \sum_j |\underline{\alpha}^j_{\mathbf{k}}|^2$ and $A_2 = \sum_j \overline{\alpha}^j_{\mathbf{k}}\underline{\alpha}^j_{\mathbf{k}}$, which, in the case of vitreous silica, give $A_1 \simeq 0.7$ and $A_2 \simeq 0.8$.

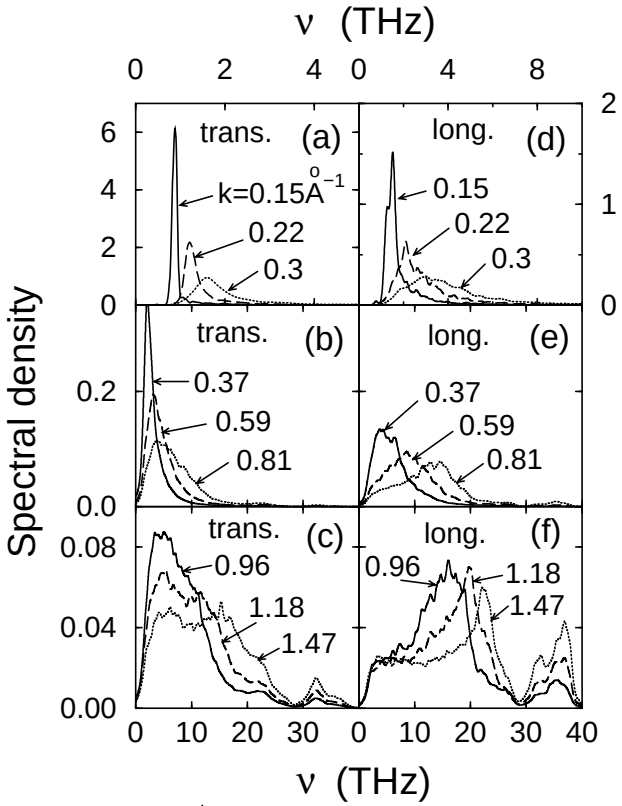

FIGURE 1. The spectral densities $|\overline{\alpha}^j_{\mathbf{k}}|^2$ for transverse ((a), (b) and (c)) and longitudinal ((d), (e) and (f)) initial polarizations for different magnitudes, k, of the initial wavevector as shown in the figure.

The shape of the spectral density depends on the characteristics of the plane wave (wavevector and polarization) and on the atomic structure itself. In disordered structures and for small values of the wavevector magnitude ($ka \ll 1$), the spectral density both for longitudinal and transverse polarizations has the shape of a single pronounced peak (see Figs. 1(a) and 1(d)). The positions of these low-frequency peaks at $\nu_{\rm t,l}$ are related to the wavevector magnitude according to the linear dispersion relation (see Fig. 2),

$$\nu_{\rm t,l} \simeq c_{\rm t,l} k/2\pi \ . \tag{22}$$

As seen from Fig. 2, the calculated dots in the low-frequency range lie on the straight lines plotted using experimental sound velocities ($c_{\rm t} \simeq 37.5 \mathring{A}$/ps and $c_{\rm l} \simeq 59 \mathring{A}$/ps [42]).

With an increase of the magnitude k of the wavevector, the peak-shaped spectral density shifts to higher frequencies and its width increases (see Figs. 1(b) and 1(e)). At large enough $k \geq 1 \mathring{A}^{-1}$, the spectral density no longer consists of a single peak but rather resembles the vibrational density of states (VDOS) (see Figs. 1(c) and 1(f)), clearly showing the two frequency bands found in v-SiO_2 [40].

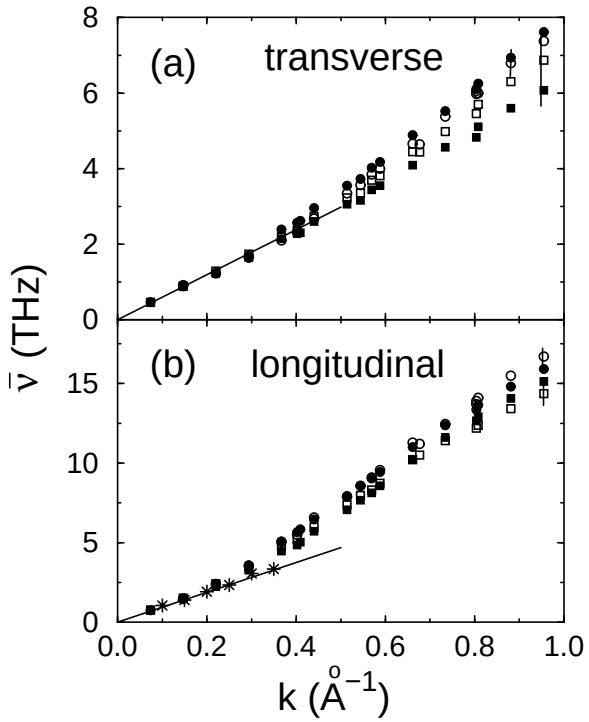

FIGURE 2. The dispersion laws for transverse (a) and longitudinal (b) polarizations of the initial plane-wave excitation. The solid circles and squares were obtained from the fit of the spectral densities by Lorentzians and the DHO model, respectively. The stars in (b) correspond to IXS data by Benassi *et al* [42]. The solid lines represent the long-wavelength limit characterized by the experimental sound velocities.

If the spectral densities are peak-shaped, two of their characteristics, the peak position and width, are normally used in order to describe the propagation of external plane-wave excitations [19,21,42,43]. The peak position is associated with the average frequency of the propagating excitation, while the peak width is associated with the decay time of the excitation. Indeed, if we look at the $\mathbf{k}$-plane-wave component in the propagating excitation, $\mathbf{u}(t)$, its evolution with time is described by relation (7) at $\mathbf{k}' = \mathbf{k}$. The weight (amplitude) of this component, $a_{\mathbf{k}}(t)$, decays with time according to Eqs. (10) and (12). A rough estimate of the time dependence of $a_{\mathbf{k}}(t)$ can be obtained if we assume that $a_{\mathbf{k}}(t) \propto a_{\mathbf{k},\mathrm{c}}(t)$, i.e. $a_{\mathbf{k}}(t)$ is approximately the back cosine Fourier transformation of the spectral density $\overline{\alpha}^j_{\mathbf{k}}\underline{\alpha}^j_{\mathbf{k}}$ (see Eq. (12)). If the spectral density has the shape of a well-defined peak which can be fitted, say, by a Lorentzian, i.e.

$$f_{\mathrm{L}} = \frac{1}{\pi}\frac{(\Gamma_\omega/2)}{(\omega - \overline{\omega}_k)^2 + (\Gamma_\omega/2)^2} \ , \tag{23}$$

where the Lorentzian position $\overline{\omega_k}$ and full-width at half-maximum (FWHM) Γ_ω are the fitting parameters, then the back cosine Fourier transform of the function (23) is

$$a_k(t) \simeq A_2 \cos\overline{\omega}_k t \exp\left\{-\Gamma_\omega t/2\right\} \ , \tag{24}$$

where we have actually used Eq. (23) to fit the spectral density $|\overline{\alpha}^j_{\mathbf{k}}|^2$ normalized to unity and then took into account the factor A_2 (see the beginning of the section). As clearly seen from Eq. (24), the decay of the $\mathbf{k}$-plane-wave component can be characterized by the average radial frequency $\overline{\omega}_k$ and the inverse decay time

$$\tau_k^{-1} \simeq \Gamma_\omega(k)/2 = \pi\Gamma_\nu(k) \ , \tag{25}$$

with $\Gamma_\nu(\mathrm{THz}) = \Gamma_\omega/2\pi$.

In Refs. [42,21], the damped harmonic oscillator (DHO) model has been used to fit spectral densities, which gives similar values for the average frequency and width, if $(\Gamma_\omega)^2 \ll \overline{\omega}_k^2$. This inequality holds true in the region $k \leq 1\mathring{A}^{-1}$ and in particular in the IR regime around $k \sim 0.1\mathring{A}^{-1}$ (see below), where the spectral densities have a well-defined peak shape and fitting of the spectral densities by Lorentzian and/or DHO curves makes sense.

We have used fits both by the Lorentzian and DHO models to obtain the average frequency and decay time (not shown, see Ref. [46] for more detail) of the propagating plane-wave excitation as a function of the initial wavevector. The dependence of $\overline{\nu}_k = \overline{\omega}_k/2\pi$ vs. k shown in Fig. 2 can be associated with some sort of "dispersion law". Of course, the propagating plane-wave excitation cannot be characterized by only one wavevector (and single frequency) and instead consists of a packet of plane waves (see Eq. (6)) with different wavevectors (packet of eigenmodes characterized by different frequencies). We chose from the $\mathbf{k}'$-packet only one component characterized by the same wavevector as that of the initial plane

wave and followed its time evolution. In that case, the dependencies $\overline{\nu}_k$ presented in Fig. 2 can be regarded as the dispersion laws for a single plane-wave component. The experimental data for longitudinal external plane-wave excitations from IXS experiments [42], obtained by fitting the experimental curves with the DHO model, are shown by the stars in Fig. 2(b) and they agree well with our results.

Note that the dispersion laws for both branches are practically linear in the low-frequency (long-wavelength) regime for $\nu \leq 3$THz. Above this frequency, a sort of "fast-sound" behaviour is observed. The increase in the slope of $\overline{\nu}_k$ is related to the changes in the shape of the spectral densities. A shoulder on the high-frequency side of the spectral-density peak for the longitudinal branch starts to appear at $k \geq 0.3\mathring{A}^{-1}$ ($\nu \geq 0.3$THz - see Figs. 1(d),(e)). A similar transformation happens with the peak for the transverse branch at $k \geq 0.5\mathring{A}^{-1}$.

B Disordered zig-zag chain

The other structural model we consider here is a toy model, namely a linear zig-zag chain on the plane. Toy models are very useful in studying atomic dynamics. Usually, scalar models are investigated because of their simplicity [34,44,45]. However, important effects related to mixing of modes of different polarizations [46] are missed in such models. That is why we consider below one of the simplest vectoral models, namely a zig-zag chain in the $x-y$ plane (see Fig. 3).

Consider a chain with 2 atoms in the unit cell: $\mathbf{r}_1^{(0)}\{x_1, y_1\}$ and $\mathbf{r}_2^{(0)}\{x_2, y_2\}$, so that the positions of the other atoms can be found as $\mathbf{r}_{i,1}^{(0)} = \mathbf{r}_1^{(0)} + i\mathbf{a}$ and $\mathbf{r}_{i,2}^{(0)} = \mathbf{r}_2^{(0)} + i\mathbf{a}$ with $i = 0, \pm 1, \ldots$, where $\mathbf{a} = \{a, 0\}$ is a unit-cell vector, so that the chain is directed along the x axis (see Fig. 3).

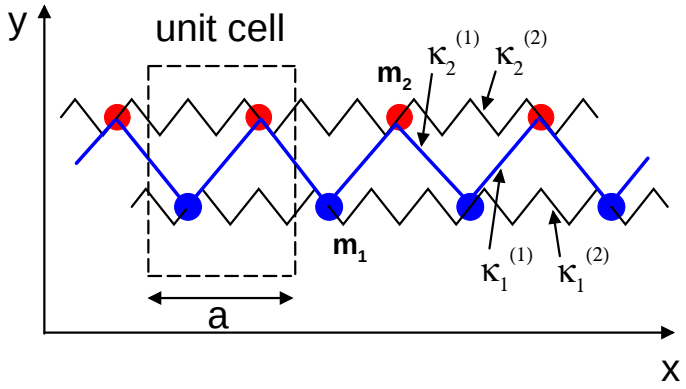

FIGURE 3. Zig-zag chain with two atoms in the unit cell.

The nearest neighbours of different types (atoms 1 and atoms 2) are connected by springs with spring constants $\kappa^{(1)}_{1,i}$ in the same unit cell i and with $\kappa^{(1)}_{2,i}$ in different unit cells (i and $i+1$), while the nearest neighbours of the same type are linked by springs with constants $\kappa^{(2)}_{1,i}$ for atoms of the first type (the lower row) and $\kappa^{(2)}_{2,i}$ for the atoms of the second type (upper row).

The potential energy then has the following expression:

$$V(\mathbf{r}_{1,1}, \mathbf{r}_{1,2}, \ldots) = \frac{1}{2}\sum_{i}^{N_{\rm uc}} \{\kappa^{(1)}_{1,i}\left(|\mathbf{r}_{i,2} - \mathbf{r}_{i,1}| - |\mathbf{r}^{(0)}_{i,2} - \mathbf{r}^{(0)}_{i,1}|\right)^2 + \kappa^{(1)}_{2,i}\left(|\mathbf{r}_{i+1,1} - \mathbf{r}_{i,2}| - |\mathbf{r}^{(0)}_{i+1,1} - \mathbf{r}^{(0)}_{i,2}|\right)^2 + \sum_{j=1,2}\kappa^{(2)}_{j,i}\left(|\mathbf{r}_{i+1,j} - \mathbf{r}_{i,j}| - |\mathbf{r}^{(0)}_{i+1,j} - \mathbf{r}^{(0)}_{i,j}|\right)^2\} \ , \quad (26)$$

with i numbering all unit cells.

Four branches occur in the dispersion relation: two acoustic (longitudinal and transverse) and two optic branches (see Fig. 4a). The analytical expression for the dispersion is available for the symmetric case ($m_1 = m_2 = m; \kappa^{(1)}_{1,i} = \kappa^{(1)}_{2,i} = \kappa^{(1)}; \kappa^{(2)}_{1,i} = \kappa^{(2)}_{2,i} = \kappa^{(2)}; x_1/a = y_1/a = 0; x_2/a = 0.5$):

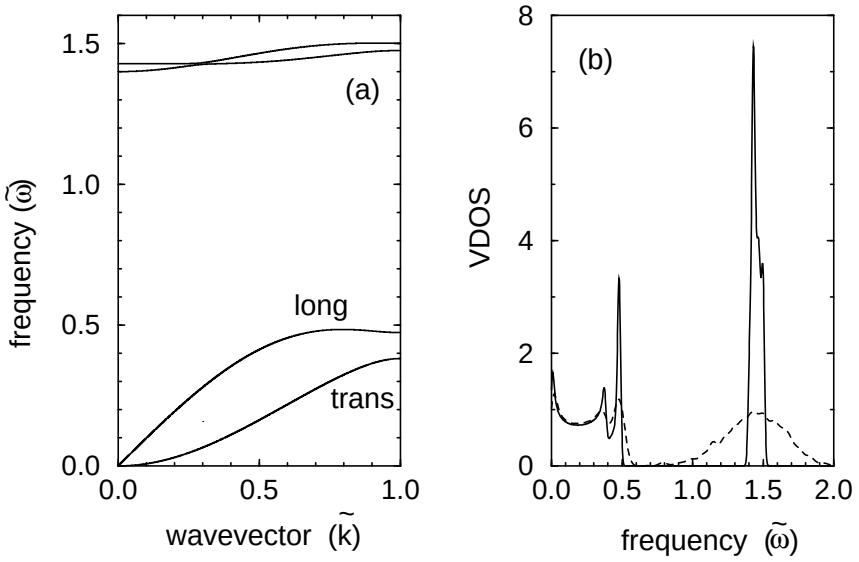

FIGURE 4. (a): Dispersion curves ($\tilde{\omega} = \omega\sqrt{m/\kappa^{(1)}}$ vs $\tilde{k} = k/(\pi/a)$) for the zig-zag chain model characterized by the following parameters: the equilibrium coordinate of atoms in the unit cell, $x_1/a = 0; y_1/a = 0$, $x_2/a = 0.4; y_2/a = 0.5$, ratio of force constants $\kappa^{(1)}/\kappa^{(2)} = 0.1$ ($\kappa^{(1,2)}_1 = \kappa^{(1,2)}_2$), masses $m_1 = m_2 = m$ and the total number of atoms $N = 2000$. (b): The VDOS of the zig-zag chain model with the same set of parameters as in (a) (solid line) together with that for a disordered chain with fluctuations in force constants $\delta\kappa^{(1)}/\kappa^{(1)} = 0.3$, $\delta\kappa^{(2)}/\kappa^{(2)} = 0.3$ (dashed line).

$$\frac{(\omega(k))^2}{(\kappa^{(1)}/m)} = 1 + \frac{A}{2} \pm \left[1 + \frac{A^2}{4} \pm A\cos\left(ka/2\right)\right]^{1/2} , \tag{27}$$

with $A = 2\left(1 - \cos\left(ka\right)\right)\left(\kappa^{(2)}/\kappa^{(1)}\right)$. From this expression it is not difficult to obtain that in the low-frequency limit ($\omega \to 0$) for the longitudinal acoustic branch not surprisingly $\omega \propto k$, while for the transverse acoustic branch $\omega \propto k^2$. Such a k^2-dependence is typical for transverse vibrations of a linear chain and is related to the much smaller restoring force in the y-direction (compared to that in the x-direction) for long-wavelength vibrations because of the absence of the spring continuum in that direction.

The vibrational density of states $g(\omega)$ contains two bands characterized by typical van Hove singularities around the band boundaries (see Fig. 4b). The k^2-dependence of the transverse acoustic branch results in an $\omega^{-1/2}$ singularity of the VDOS as the frequency approaches zero, $\omega \to 0$.

We are interested mainly in disordered structures. Several different types of disorder can be introduced in the system:

(i) Positional disorder which is due to random positional vectors $\mathbf{r}_i^{(0)}$.

(ii) Force-constant disorder: κ_i are randomly distributed around their mean value, $\overline{\kappa}$,

$$\kappa_i = \overline{\kappa} + \delta\kappa \cdot \delta_{i,\mathrm{ran}} , \tag{28}$$

where $\delta\kappa$ is a typical width of the distribution and $\delta_{i,\mathrm{ran}}$ are random numbers distributed around zero with the density distribution, $\rho(\delta)$, e.g. the normal distri-

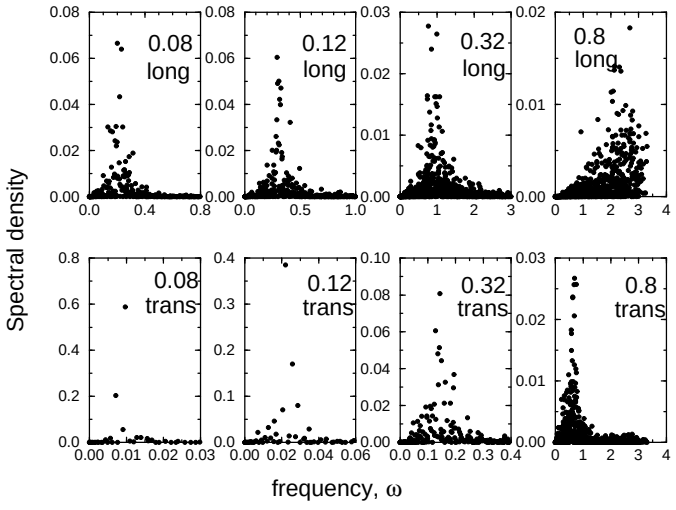

FIGURE 5. Spectral densities for a disordered zig-zag chain described by the following parameters: $m_1 = m_2 = 1, \delta m_1 = \delta m_2 = 0$, $\kappa^{(1)} = \kappa^{(2)} = 1, \delta\kappa^{(1)} = \delta\kappa^{(2)} = 1.0$, $x_1/a = y_1/a = 0, x_2/a = y_2/a = 0.5, a = 1$ and $N = 1000$. The wavevector magnitude, k, and polarizations (longitudinal or transverse) of the initial plane wave are marked in the figure.

bution, $\rho(\delta) = \exp\{-\delta^2/2\}/\sqrt{2\pi}$, with unit variance. Possible negative values of the spring constants are replaced by their absolute values.

(iii) Mass disorder: the atomic masses are randomly distributed, $m_i = \overline{m} + \delta m \cdot \delta_{i,\mathrm{ran}}$.

In the case of force-constant and mass disorder (which are considered in what follows), the equilibrium positions of the atoms are not changed. This is quite convenient and an ideal (crystalline) linear chain can be treated as the crystalline counterpart of the disordered chain.

The VDOS of a disordered zig-zag chain is similar to that for the crystalline chain (see Fig. 4b) except all sharp features (excluding the region around zero) are washed out (band tails appear). We should also note that extra states (relative to the Debye spectrum) appear in the low-frequency regime ($\omega \leq c_{\mathrm{t,l}}(\pi/a)$, with $c_{\mathrm{t,l}}$ being the transverse or longitudinal sound velocity. These extra states, characterized by the change in the VDOS, $\Delta g(\omega) = g(\omega) - g_{\mathrm{cryst}}(\omega)$, are called the boson peak [40].

The spectral densities for the disordered zig-zag chain, being of particular interest, are calculated according to Eq. (3) and presented in Fig. 5.

As expected in the long-wavelength limit, the spectral density has the shape of a peak. The position of the peak can be approximately found from the dispersion for acoustic branches (see below). The width of the peak increases with increasing magnitude of the wavevector of the initial plane wave. This corresponds to more intense scattering of the plane waves by disorder.

IV ANALYSIS OF THE FINAL STATE IN MOMENTUM SPACE

As is well known, a scattering process can be investigated by analysis of the final state. First, we consider the final state of a single $\mathbf{k}$-plane-wave component characterized by the same wavevector as the initial one. The phase of this wave has a random value and is not an informative characteristic. The important quantity is the amplitude of the wave, or more precisely its squared average value, defined by Eq. (18) with $\mathbf{k}' = \mathbf{k}$,

$$\overline{a_{\mathbf{k}}^2} = \frac{1}{2}\left\{ \frac{\sum_j |\overline{\alpha}_{\mathbf{k}}^j|^2 |\underline{\alpha}_{\mathbf{k},\mathrm{s}}^j|^2}{(\langle \mathbf{w}_{\mathbf{k},\mathrm{s}}^2 \rangle)^2} + \frac{\sum_j |\overline{\alpha}_{\mathbf{k}}^j|^2 |\underline{\alpha}_{\mathbf{k},\mathrm{c}}^j|^2}{(\langle \mathbf{w}_{\mathbf{k},\mathrm{c}}^2 \rangle)^2} \right\} \simeq \frac{\sum_j |\overline{\alpha}_{\mathbf{k}}^j|^2 |\underline{\alpha}_{\mathbf{k}}^j|^2}{(\langle \mathbf{w}_{\mathbf{k}}^2 \rangle)^2} \ . \tag{29}$$

This value can be easily estimated for a peak-shaped spectral density of width Γ. Indeed, the number of eigenmodes contributing to an initial plane wave is of order $3N \cdot (\Gamma/D)$, where D is the width of the whole vibrational spectrum ($\simeq 40$THz in the case of vitreous silica). Then we can easily evaluate from the normalization conditions Eqs. (5), (17) for the spectral densities the average value of the spectral density in the peak region, $|\overline{\alpha}_{\mathbf{k}}^j|^2 \sim |\underline{\alpha}_{\mathbf{k},\mathrm{s}}^j|^2 \sim (D/\Gamma) \cdot (1/3N)$, and obtain the following estimate for $\overline{a_{\mathbf{k}}^2}$,

$$\overline{a_{\mathbf{k}}^2} \sim \frac{D}{\Gamma} \cdot \frac{1}{3N} \ , \tag{30}$$

where we have taken into account that $\langle \mathbf{w}_{\mathbf{k}}^2 \rangle \sim 1$ according to Eq. (5). The factor D/Γ in relation (30) shows that the averaged squared amplitude is inversely proportional to the number of initially excited modes and not to all the modes. The factor D/Γ in the Ioffe-Regel (IR) region is much larger than unity; $D/\Gamma \sim 10^2$ for $\Gamma \sim \nu_{\rm IR}/\pi \sim 0.3$THz. Therefore we can say that the $\mathbf{k}$-plane-wave component around and below the IR regime is not damped (the squared average amplitude is not of order $1/3N$) but rather is attenuated (scattered), weakly (strongly) below (beyond) the IR limit as discussed below. The $\mathbf{k}$-plane-wave component is damped at $k \geq k_* \simeq 1\mathring{A}^{-1}$ when the peak width becomes comparable to the full spectral width, $\Gamma \sim D$.

The analysis of all $\mathbf{k}'$-plane-wave components in the final state, in particular the distribution (18) of their weights, allows the scattering mechanism to be clarified. Let us consider an initial plane wave characterized by the wavevector $\mathbf{k}$ and polarization $\hat{\mathbf{n}}$. This wave is scattered with time into different plane waves characterized by wavevectors $\mathbf{k}'$ and polarizations $\hat{\mathbf{n}}'$, which do not necessarily coincide with the initial polarization. We would like to know the weights of all plane-wave components in the final state as a function of the wavevector magnitude k'. The distributions of the transverse and longitudinal plane waves, $\rho(\mathbf{k}', \hat{\mathbf{n}}'_{\rm t}|\mathbf{k}, \hat{\mathbf{n}})$ and $\rho(\mathbf{k}', \hat{\mathbf{n}}'_{\rm l}|\mathbf{k}, \hat{\mathbf{n}})$ (see Eq. (19)), and the distribution averaged over polarizations, $\rho_{\rm av}(\mathbf{k}'|\mathbf{k}, \hat{\mathbf{n}})$ (see Eq. (20)), for both transverse $\hat{\mathbf{n}}_{\rm t}$ and longitudinal $\hat{\mathbf{n}}_{\rm l}$ polarizations of the initial plane-wave excitation are of particular interest. These distributions depend only on the spectral densities $|\overline{\alpha}_{\mathbf{k}}^j|^2$, $|\underline{\alpha}_{\mathbf{k}'}^j|^2$ and the vibrational spectrum itself, and can be easily calculated numerically for different k.

A Vitreous silica

The results of such calculations for vitreous silica are presented in Fig. 6. The upper (lower) row describes the scattering of initial longitudinal (transverse) plane waves, characterized by different wavevector magnitudes, into transverse and longitudinal plane waves and also the distribution of the weights averaged over the polarization in the final state.

First, we consider scattering of a longitudinal initial wave (the upper row in Fig. 6). The weight distributions, $\rho(\mathbf{k}', \hat{\mathbf{n}}'_{\rm l}|\mathbf{k}, \hat{\mathbf{n}}_{\rm l})$ and $\rho(\mathbf{k}', \hat{\mathbf{n}}'_{\rm t}|\mathbf{k}, \hat{\mathbf{n}}_{\rm l})$, characterize the scattering of the longitudinal wave to a longitudinal wave, the $\{l \to l\}$ channel, and of the longitudinal wave to a transverse wave, the $\{l \to t\}$ channel, respectively. As follows from Fig. 6, these distributions are peak shaped but the positions of the peaks are different. The distribution for the $\{l \to l\}$ channel has a maximum around $k'_{\rm ll} \simeq k_{\rm l} \equiv k$ (or maybe a bit below the initial wavevector), while the distribution for the $\{l \to t\}$ channel is mainly concentrated at a higher wavevector value, $k'_{\rm lt} > k_{\rm l}$. The distribution, $\rho_{\rm av}(\mathbf{k}'|\mathbf{k}, \hat{\mathbf{n}}_{\rm l})$, averaged over polarizations of the final state is a sum of double the distribution for the $\{l \to t\}$ channel plus the

distribution for the $\{l \to l\}$ channel. If the peaks related to the individual channels and constituting the average distribution are narrow enough, then the distribution function $\rho_{\rm av}(\mathbf{k}'|\mathbf{k}, \hat{\mathbf{n}}_{\rm l})$ is doubly peaked (not clearly seen in Fig. 6). If the peaks are too wide, then $\rho_{\rm av}(\mathbf{k}'|\mathbf{k}, \hat{\mathbf{n}}_{\rm l})$ looks like a single wide peak (see Fig. 6) with a maximum position $k'_{\rm l,av}$ close to $k'_{\rm lt}$.

Such a shape of the distributions of the weights of plane waves in the final state can be qualitatively understood in the following way. The distribution function $\rho(\mathbf{k}', \hat{\mathbf{n}}'_{\rm t}|\mathbf{k}, \hat{\mathbf{n}}_{\rm l})$ of the transverse waves is an integral (sum in the case of a finite-size model) of the product of two spectral densities, $|\overline{\alpha}^j_{\mathbf{k},\hat{\mathbf{n}}_{\rm l}}|^2$ for longitudinal and $|\underline{\alpha}^j_{\mathbf{k}',\hat{\mathbf{n}}'_{\rm t}}|^2$ for transverse polarization. Around the IR region and below it, these peak-shaped spectral densities have maxima at $\nu_{\rm l} \simeq c_{\rm l}k/2\pi$ and $\nu'_{\rm t} \simeq c_{\rm t}k'/2\pi$, respectively, which generally do not coincide with each other. Therefore, the distribution $\rho(\mathbf{k}', \hat{\mathbf{n}}'_{\rm t}|\mathbf{k}, \hat{\mathbf{n}}_{\rm l})$ has a maximum around $k'_{\rm lt}$ satisfying the equation, $\nu_{\rm l} \simeq c_{\rm l}k/2\pi \simeq c_{\rm t}k'_{\rm lt}/2\pi \simeq \nu'_{\rm t}$, i.e.

$$k'_{\rm lt} \simeq c_{\rm l}k/c_{\rm t} \ , \tag{31}$$

which is obviously greater than the wavevector of the initial longitudinal wave.

The distribution of longitudinal waves for the $\{l \to l\}$ channel can be analysed in a similar manner. The main difference from the $\{l \to t\}$ channel is that the spectral density of the longitudinal plane wave in the final state coincides with the spectral density of the initial longitudinal plane wave at approximately the same wavevector magnitude as for the initial wave,

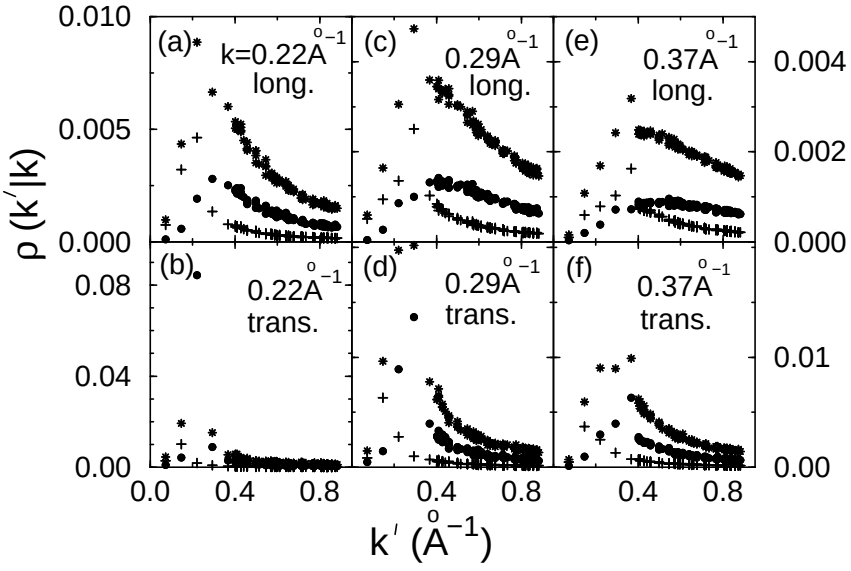

FIGURE 6. The distribution functions $\rho(\mathbf{k}', \hat{\mathbf{n}}'_{\rm t}|\mathbf{k}, \hat{\mathbf{n}})$ (circles), $\rho(\mathbf{k}', \hat{\mathbf{n}}'_{\rm l}|\mathbf{k}, \hat{\mathbf{n}})$ (pluses) and $\rho_{\rm av}(\mathbf{k}'|\mathbf{k}, \hat{\mathbf{n}})$ (stars) for longitudinal ((a), (c) and (e)) and transverse ((b), (d) and (f)) initial polarizations of plane waves characterized by different initial wavevector magnitudes k for a structural model of v-SiO_2.

$$k'_{\rm ll} \simeq k \ . \tag{32}$$

Actually, the value $k'_{\rm ll}$ should be slightly shifted to lower values, because the height of the peak for the spectral density $|\underline{\alpha}^j_{\mathbf{k}'}|^2$ increases with decreasing k' and the maximum of the product of the spectral densities is reached in the low-frequency tail of the spectral density for the initial plane wave.

The scattering of an initially transverse plane wave occurs similarly. In particular, the conclusion that the average frequency, ν', of the majority of the plane-wave components comprising the final state coincides with the average frequency, ν, of the initial plane wave,

$$\nu' \simeq \nu \ , \tag{33}$$

holds true independently of the polarization of the initial plane-wave excitation. Therefore, we can roughly say that the disorder-induced scattering of the plane wave is approximately "elastic" (on average). This is not an absolutely precise conclusion because, first, the plane-wave components are distributed in frequency (composed of eigenmodes having different frequencies) in the initial and final states and, second, even the maximum of the distribution in the final state is slightly shifted to lower frequencies as compared to the initial one, as discussed above.

In the case of the scattering of an initial transverse plane wave, two channels are available: $\{t \to l\}$ and $\{t \to t\}$. The distribution functions, $\rho(\mathbf{k}', \hat{\mathbf{n}}'_{\rm l}|\mathbf{k}, \hat{\mathbf{n}}_{\rm t})$ and $\rho(\mathbf{k}', \hat{\mathbf{n}}'_{\rm t}|\mathbf{k}, \hat{\mathbf{n}}_{\rm t})$, of the weights of plane waves in the final state for these channels have peaks located around the following values:

$$k'_{\rm tl} \simeq c_{\rm t}k/c_{\rm l} \quad \text{and} \quad k'_{\rm tt} \simeq k \ . \tag{34}$$

As follows from Eq. (34) and Figs. 6(b),(d),(f), the peak for longitudinal waves lies below the initial k, while for transverse waves the peak approximately coincides with k, being slightly shifted to smaller values for reasons similar to those discussed above for the $\{l \to l\}$ channel.

The distribution functions shown in Fig. 6 were obtained for a bar-shaped structural model of v-SiO_2. Such a model is effectively one-dimensional and has restrictions for the available initial $\mathbf{k}$ and final $\mathbf{k}'$ vectors, which are mainly directed along the bar in the low-k limit. This also restricts the number of scattering channels. In order to check the influence of the dimensionality of the model on the scattering of plane waves, we have performed a similar analysis for a cubic (3-dimensional) model of v-SiO_2 and have not found any influence of the dimensionality of the model for the available wavevector magnitudes $k \geq 0.22\mathring{A}^{-1}$ (for the cubic model).

Poor statistics in the long-wavelength limit (see Fig. 6) is a finite-size effect related to the restricted number of the wave-vectors allowed by the periodic boundary conditions. An analytical extrapolation approach [46] can be used to overcome such a shortcoming.

B Zig-zag chain

Another possible way to overcome the disadvantages of finite-size 3-D numerical models is to analyse low-dimensional models. Much lower wavevectors $k \geq k_{\min}^{(d)} = 2\pi/N^{1/d}a$ are available, for example, in one-dimensional ($d = 1$) models as compared to the 3-D case, and the acoustic spectrum appears to be be much more dense. In order to check and support the analytical and numerical approaches presented above for the 3-D case, we have performed numerical experiments for a disordered 1-D zig-zag chain (see Sec. III B) and calculated the distribution function $\rho(\mathbf{k}', \hat{\mathbf{n}}'|\mathbf{k}, \hat{\mathbf{n}})$ for it.

Our main purpose here is to calculate the distribution function $\rho(\mathbf{k}', \hat{\mathbf{n}}'|\mathbf{k}, \hat{\mathbf{n}})$ characterizing the scattering of a plane-wave excitation. First, we have calculated this distribution function for the crystalline counterpart ($\delta\kappa_i = 0$) and not surprisingly we found for $k \leq \pi/a$ only $\{t \to t\}$ and $\{l \to l\}$ channels (see the lower row in Fig. 7 marking the peaks at $k'_{\rm tt} = k$ and $k'_{\rm ll} = k$ for the $\{t \to t\}$ and $\{l \to l\}$ channels, respectively). Disorder changes the situation dramatically and gives rise to the occurrence of $\{t \to l\}$ and $\{l \to t\}$ channels (see the upper row in Fig. 7), in complete agreement with the results of the k-analysis given in Fig. 6 for the case of v-SiO_2. The positions of the additional peaks, at $k'_{\rm tl}$ ($\{t \to l\}$ channel), and $k'_{\rm lt}$ ($\{l \to t\}$ channel) can be obtained from the dispersion laws for the crystalline zig-zag chain by solving the equations:

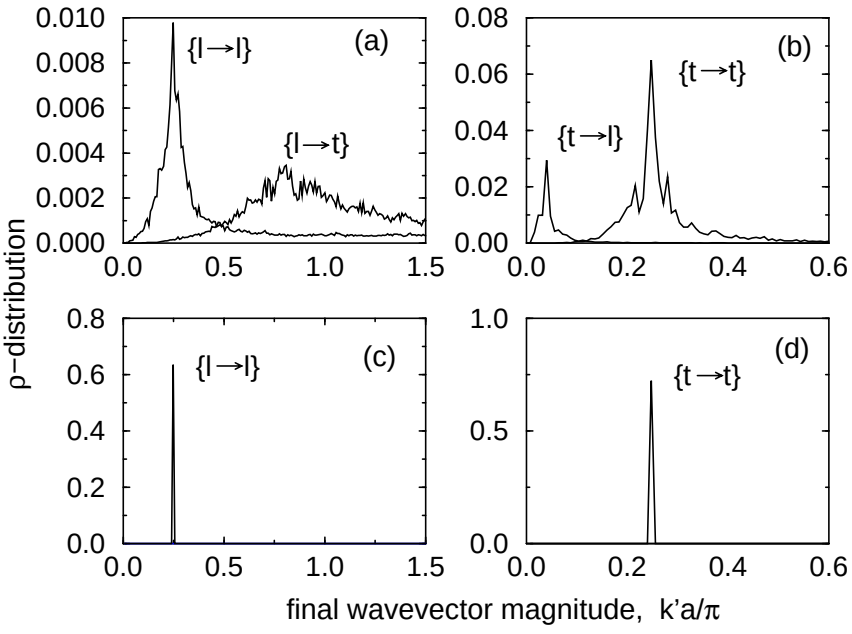

FIGURE 7. The distribution function $\rho(\mathbf{k}', \hat{\mathbf{n}}'|\mathbf{k}, \hat{\mathbf{n}})$ for different scattering channels (as marked in the figure) for a disordered ((a) and (b)), $\delta\kappa^{(1)} = \delta\kappa^{(2)} = 1$, $\delta m_1 = \delta m_2 = 0$) and an ordered ((c) and (d)) zig-zag chain characterized by the following parameters: $m_1 = m_2 = 1$, $\kappa^{(1)} = \kappa^{(2)} = 1$, $x_1/a = y_1/a = 0$, $x_2/a = y_2/a = 0.5$. The initial wavevector magnitude $ka/\pi = 0.25$.

$$\omega_{\rm t}(k) = \omega_{\rm l}(k'_{\rm tl}) \ , \tag{35}$$

and

$$\omega_{\rm l}(k) = \omega_{\rm t}(k'_{\rm lt}) \ , \tag{36}$$

respectively (see arrows in Fig. 8). The width of the peaks increases with increasing disorder. We have also found a similar shape of the distribution function ρ (for four channels) for all wavevectors $k \leq \pi/a$ with the corresponding $\omega_{\rm t}$ and $\omega_{\rm l}$ lying in the range of the dense spectrum.

V SCATTERING MECHANISM

From numerical calculations for both the 1-D zig-zag chain model and the 3-D model of v-SiO_2, we have found that plane waves scatter not only to modes of approximately the same wavelength (and polarization) but also to modes of different wavelength (and polarization) but of similar frequency. The reason for such scattering is a natural question.

In our simulations on zig-zag chains, we have found the $\{t \to l\}$ and $\{l \to t\}$ scattering channels even for models not showing an appreciable increase of the VDOS in the low-frequency regime. Hence, the appearance of the $\{t \to l\}$ and $\{l \to t\}$ channels should be explained in terms of existing transverse and longitudinal acoustic waves. Indeed, in the crystal, transverse and longitudinal acoustic phonons are orthogonal to each other, and hence transverse (longitudinal) plane waves cannot be scattered into longitudinal (transverse) plane waves (as we checked numerically; see the lower row in Fig. 7). Disorder leads to changes in the interaction energy,

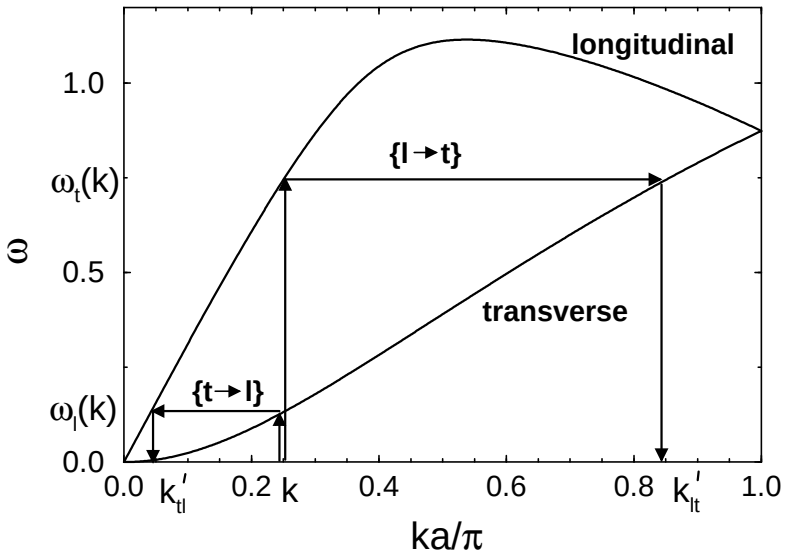

FIGURE 8. The acoustic branches for an ordered zig-zag chain characterized by the same parameters as in Fig. 7. The construction used to estimate values of $k'_{\rm tl}$ and $k'_{\rm lt}$ is shown.

with the result that an acoustic phonon with a particular energy can couple to other phonons with closely comparable energies, including phonons with different polarizations and wavevectors. Therefore, the resulting eigenmodes contain components of different polarization and different wavevectors. A plane wave is not an eigenmode in the disordered stucture and it is scattered into eigenmodes of approximately the same energy as that of the plane wave. These eigenmodes contain both transverse and longitudinal components and therefore an original plane wave, independent of its polarization, is scattered into both transverese and longitudinal plane waves. This gives a qualitative explanation of the existence of $\{t \rightarrow l\}$ and $\{l \rightarrow t\}$ scattering channels.

In the 3-D case, the situation can be more complicated. Apart from the scattering mechanism due to the disorder-induced mixing of transverse and longitudinal plane waves discussed above, extra states (comprising the Boson peak) relative to the Debye spectrum (e.g. optic modes pushed down by disorder (see [46,47])) could participate in the hybridization between plane waves with different polarization.

REFERENCES

1. *Scattering and Localization of Classical Waves in Random Media*, edited by Sheng P. (World Scientific, Singapore, 1990).
2. Sheng P., *Introduction to Wave Scattering, Localization, and Mesoscopic Phenomena* (Academic Press, San Diego, 1995).
3. Mott N.F. and Davis E.A., *Electronic Processes in Non-Crystalline Materials* , 2nd ed. (Clarendon Press, Oxford, 1979).
4. John S., Sompolinsky H., and Stephen M.J., Phys.Rev. B **27**, 5592 (1983).
5. Aharony A., Alexander S., Entin-Wohlman O., and Orbach R., Phys. Rev. Lett. **58**, 132 (1987).
6. Alexander S., Phys.Rev. B **40**, 7953 (1989).
7. Ioffe A.F. and Regel A.R., Prog. Semicond. **4**, 237 (1960).
8. Sheng P., Zhou M., and Zhang Z.-Q., Phys. Rev. Lett. **72**, 234 (1994).
9. Anglaret E., Hasmy A., Courtens E., Pelous J., and Vacher R., Europhys. Lett. **28**, 591 (1994).
10. Grest G.S., Nagel S.R., and Rahman A., Phys. Rev. Lett. **49**, 1271 (1982).
11. Hafner J. and Crajci M., J.Phys.: Cond.Matter,**6**, 4631 (1994).
12. Schober H.R. and Laird B.B., Phys. Rev. B **44**, 6746 (1991).
13. Gurevich V.L., Parshin D.A, Pelous J., and Schober H.R., Phys.Rev., B **48**, 16318 (1993).
14. Mazzacurati V., Ruocco G., and Sampoli M., Europhys.Lett., **34**, 681 (1996).
15. Sampoli M., Benassi P., Dell'Anna R., Mazzacurati V. and Ruocco G., Phil.Mag., B **77**, 473 (1998).
16. Taraskin S.N. and Elliott S.R., Europhys. Lett., **39**, 37 (1997).
17. Ribeiro M.C.C., Wilson M., and Madden P.A., J.Chem.Phys., **108**, 9027 (1998).
18. Allen P.B. and Feldman J.L., Phys. Rev. B **48**, 12581 (1993),

19. Feldman J.L., Kluge M.D., Allen P.B., and Wooten F., Phys. Rev. B **48**, 12589 (1993).
20. Fabian J. and Allen P.B., Phys. Rev. Lett., **77**, 3839 (1996).
21. Dell'Anna R., Ruocco G., Sampoli M., and Viliani G., Phys. Rev. Lett. **80**, 1236 (1998).
22. Feldman J.L., Allen P.B., and Bickham S.R., Phys. Rev. B **59**, 3551 (1999).
23. Wischnewski A., Buchenau U., Dianoux A.J., Kamitakahara W.A., and Zarestky J.L., Phys. Rev. B **57**, 2663 (1998).
24. Sheng P. and Zhou M., Science **253**, 539 (1991).
25. Buchenau U., Galperin Yu.M., Gurevich V.L., Parshin D.A., Ramos M.A. and Schober H.R., Phys.Rev., B **46**, 2798 (1992).
26. Gaganidze E., Konig R., Esquinazi P., Zimmer K., and Burin A., Phys. Rev. Lett. **79**, 5038 (1997).
27. Vacher R., Pelous J., and Courtens E., Phys. Rev. B **56**, R481 (1997).
28. Horbach J., Kob W. and Binder K., J.Non-Cryst.Sol., **235**, 320 (1998).
29. Maradudin A.A., Montroll E.W., Weiss G.H., and Ipatova I.P., *Theory of Lattice Dynamics in the Harmonic Approximation* (Acad. Press, N.Y., 1971).
30. Leibfried G. and Breuer N., *Point Defects in Metals I. Introduction to the theory* (Springer, Berlin, 1978).
31. Dederichs P.H. and Zeller R., in *Point Defects in Metals II. Dynamical Properties and Diffusion Controlled Reactions* (Springer, Berlin, 1980).
32. Klinger M.I., Phys.Rep., **165**, 275 (1988).
33. Galperin Yu.M., Karpov V.G., and Kozub V.I., Adv.Phys. **38**, 669 (1989).
34. Schirmacher W., Diezemann G., and Ganter C., Phys. Rev. Lett. **81**, 136 (1998).
35. Elliott S.R., *Physics of Amorphous Materials* 2^{nd} Edn. (Longman, N.Y., 1990).
36. Hansen J.-P. and McDonald I.R., *Theory of Simple Liquids* 2-nd Ed. (Academic Press, London, 1990).
37. van Beest B.W.H., Kramer G.J., and van Santen R.A., Phys.Rev.Lett., **64**, 1955 (1990).
38. Guissani Y. and Guillot B., J.Chem.Phys., **104**, 7633 (1995).
39. Vollmayr K., Kob W., and Binder K., Phys.Rev., **B54**, 15808 (1996).
40. Taraskin S.N. and Elliott S.R., Phys.Rev., B**56**, 8605 (1997).
41. Fernandez-Perera R., Bermejo F.J., and Enciso E., Phys. Rev., B **53**, 6215 (1996).
42. Benassi P., Krisch M., Masciovecchio C., Mazzacurati V., Monaco G., Ruocco G., Sette F., and Verbeni R., Phys. Rev. Lett. **77**, 3835 (1996).
43. Foret M., Courtens E., Vacher R., and Suck J.-B., Phys. Rev. Lett. **77**, 3831 (1996).
44. Nakayama T., Phys. Rev. Lett. **80**, 1244 (1998).
45. Parshin D.A. and Schober H.R., Phys. Rev., B **57**, 10232 (1998).
46. Taraskin S.N. and Elliott S.R., J.Phys.: Cond.Matter, **11**, A219 (1999).
47. Taraskin S.N. and Elliott S.R., Phys.Rev., B, **59**, 8572 (1999) .